A Study of Multiplicative Watermark Detection in the Contourlet Domain Using Alpha-Stable Distributions

Hamidreza Sadreazami, *Student Member, IEEE*, M. Omair Ahmad, *Fellow, IEEE*, and M. N. S. Swamy, *Fellow, IEEE*

***Abstract*— In the past decade, several schemes for digital image watermarking have been proposed to protect the copyright of an image document or to provide proof of ownership in some identifiable fashion. This paper proposes a novel multiplicative watermarking scheme in the contourlet domain. The effectiveness of a watermark detector depends highly on the modeling of the transform-domain coefficients. In view of this, we first investigate the modeling of the contourlet coefficients by the alpha-stable distributions. It is shown that the univariate alpha-stable distribution fits the empirical data more accurately than the formerly used distributions, such as the generalized Gaussian and Laplacian, do. We also show that the bivariate alpha-stable distribution can capture the across scale dependencies of the contourlet coefficients. Motivated by the modeling results, a blind watermark detector in the contourlet domain is designed by using the univariate and bivariate alpha-stable distributions. It is shown that the detectors based on both of these distributions provide higher detection rates than that based on the generalized Gaussian distribution does. However, a watermark detector designed based on the alpha-stable distribution with a value of its parameter α other than 1 or 2 is computationally expensive because of the lack of a closed-form expression for the distribution in this case. Therefore, a watermark detector is designed based on the bivariate Cauchy member of the alpha-stable family for which $\alpha = 1$. The resulting design yields a significantly reduced-complexity detector and provides a performance that is much superior to that of the GG detector and very close to that of the detector corresponding to the best-fit alpha-stable distribution. The robustness of the proposed bivariate Cauchy detector against various kinds of attacks, such as noise, filtering, and compression, is studied and shown to be superior to that of the generalized Gaussian detector.**

***Index Terms*— Digital image watermarking, multiplicative watermark, contourlet transform, alpha-stable family of distributions.**

I. Introduction

DIGITAL data distribution on the internet has made researchers to pay special attention to copyright issues. Digital watermarks have been widely applied to different media contents such as videos, audios and images for the purpose of identifying the ownership [1]–[4]. Various watermarking schemes have been proposed to protect the copyright information. They may be categorized in many ways such as the domain in which the watermark is embedded for example pixel [5], frequency [6]–[12] or hybrid [13], and the method of embedding, additive [6], [7], [9], [10], [14], [15], multiplicative [11], [12], [16]–[20] or based on quantization [21], [22]. In many applications, the detection of a specific watermark is sufficient [7]–[11], [17], [18], without it being extracted. The commonly-used additive and multiplicative embedding rules are as: additive watermarking $Y = X + \zeta W$ and multiplicative watermarking $Y = X + \zeta XW$, where X and Y are, respectively, the original and watermarked data, W is a watermark sequence and ζ is a weighting factor that controls the strength of the watermark. It should be mentioned that by increasing ζ, the robustness of the watermarking scheme is increased. However, the extent to which one can increase the watermark strength depends on the properties of the human visual system (HVS) [23]–[25], which guarantees the imperceptibility of the watermarking scheme. In view of the robustness, the multiplicative watermarks have been widely used for copyright protection. Hence, detection of multiplicative watermarks has received a great deal of attention [11], [12], [20]. Due to their simplicity, correlation-based detectors have been used for detecting the watermarks, especially for additive watermarking schemes [2], [13], [21]. However, it has been shown that these detectors are not optimal for the detection of multiplicative watermarks [12].

A watermarking scheme should be robust against any intentional or unintentional distortion and the authorized user should be able to detect the watermark. The robustness can be significantly increased by utilizing the spread spectrum technique [3], [18], [26] in which the watermark is embedded in a transformed domain such as the discrete Fourier transform [2], [8], [11], discrete cosine transform [6], [7], [10], discrete wavelet transform [15], [21], [22], [24], or the contourlet transform [24], [27]–[33]. Recently, a number of watermarking schemes have been proposed, wherein the watermark is embedded into the contourlet coefficients of the image. There have been several works suggesting that the performance of the contourlet-domain algorithms is resistant to attacks than those based on other frequency-domain watermarking algorithms such as the wavelets [30]–[32]. This is mostly

Manuscript received April 25, 2014; accepted July 3, 2014. Date of publication July 16, 2014; date of current version September 2, 2014. This work was supported in part by the Natural Sciences and Engineering Research Council of Canada and in part by the Regroupement Strategique en Microelectronique du Quebec. The associate editor coordinating the review of this manuscript and approving it for publication was Prof. Stefano Tubaro.

The authors are with the Center for Signal Processing and Communications, Concordia University, Montreal, QC H3G 1M8, Canada (e-mail: h_sadrea@encs.concordia.ca; omair@encs.concordia.ca; swamy@encs.concordia.ca).

Color versions of one or more of the figures in this paper are available online at http://ieeexplore.ieee.org.

Digital Object Identifier 10.1109/TIP.2014.2339633

due to the spreading property of the contourlet transform in that if the watermark bits are inserted into specific subbands (e.g., lowpass or highpass), they will be spread out into all the subbands when the watermarked image is reconstructed [24]. The most commonly used detector for the frequency domain watermarking schemes is the correlation detector, which is optimal only if the data samples follow the Gaussian distribution function [34]. If these data samples are not Gaussian, optimal or sub-optimal detectors are developed by modeling the frequency domain coefficients using various PDFs, such as the Laplacian [22], [35] Student-t [36], and generalized Gaussian [6], [12], [33], [37], [38]. In view of the fact that the contourlet coefficients of an image are highly non-Gaussian [33], [37]–[39], i.e., having large peaks and tails heavier than that of a Gaussian PDF, a proper distribution to model the statistics of the contourlet coefficients would be a heavy-tailed PDF. It has been shown in [33] and [39] that the generalized Gaussian distribution can model the contourlet coefficients. Accordingly, a statistical watermark detector has been proposed in [33] for the contourlet-domain image watermarking that models the contourlet coefficients by the GG distribution. The bivariate distributions have been used for modeling the wavelet transform coefficients in various image processing applications, particularly in image denoising [40], [41]. Wavelet coefficients of color images have been modeled by using multivariate power-exponential distribution in [42], which focuses on dependencies between RGB channels. However, there does not exist any work in image watermarking for modeling the across-scale dependencies of the contourlet coefficients using a bivariate distribution.

In this work, we first explore the modeling of the contourlet coefficients by the alpha-stable family of distributions. Through a comprehensive modeling of actual data, it is shown that the contourlet-domain subband decomposition of real images have significant non-Gaussian statistics that are best described by families of heavy-tailed distributions, such as the alpha-stable family. It should be pointed out that we consider both the univariate and bivariate statistical models to thoroughly investigate the modeling of the contourlet coefficients. It is shown that the univariate and bivariate alpha-stable distributions can accurately model the heavy-tailed properties of the contourlet coefficients both in terms of the objective measure of Kolmogorov-Smirnov distance and subjective measure of comparing the histograms of various distributions. In addition, it is shown that the bivariate alpha-stable distribution can capture the across scale dependencies of the contourlet coefficients. Encouraged by the modeling results, statistical watermark detectors are designed in the contourlet domain by using both the univariate and bivariate alpha-stable distributions and their performances are evaluated numerically by obtaining the receiver operating characteristics. Since the bivariate Cauchy PDF is a particular case of the alpha-stable distributions having a closed form expression for its PDF, we will also study the performance of the detector using this distribution, since we expect it to have a much lower computational complexity. The robustness of the proposed watermarking scheme is then examined when the watermarked images are attacked by JPEG compression, additive white Gaussian noise, salt & pepper noise and median filtering. Finally, we compare the performance of the proposed detector with that of the GG detector.

The paper is organized as follows: Sections II presents the contourlet transform, the alpha-stable distribution and results on modeling of contourlet coefficients of the test images using this distribution. In Section III, watermark embedding procedure is discussed and a blind watermark detector constructed. In Section IV, the performance of the proposed watermarking detector is examined in terms of the probabilities of detection and false alarm and then compared to that of the GG detector.

II. Data Modeling

A. Contourlet Transform

The contourlet transform, a new image decomposition scheme proposed in [40], provides an efficient representation for 2D signals with smooth contours and in this case outperforms the wavelet transform which fails to recognize the smoothness of the contour. The contourlet transform has also the multiscale and time-frequency localization features of the wavelet transform. In addition it offers a higher degree of directionality with better sparseness. Further, due to using iterated filter banks, it is computationally efficient. There are number of other structures such as the dual-tree complex wavelet [44], ridgelet [26], [45] and curvelet [46], [47] that also provide multiscale and directional image representation. However, the contourlet transform can provide a flexible number of directions in each subband. In this regard, this transform is superior to the wavelet and the complex wavelet transforms. Compared to the curvelet transform, the contourlet transform is preferred, since it is defined on rectangular grids and offers a seamless translation to the discrete world [40]. Moreover, the contourlet transform has a 2D frequency partitioning on concentric rectangles rather than on concentric circles for the curvelet, and hence overcome the blocking artifact deficiency of the curvelet transform.

B. Alpha-Stable Distributions

It is known that the contourlet coefficients of images have non-Gaussian property and heavy tails. In view of this, an appropriate distribution to model the statistics of the contourlet coefficients would be the one having large peaks, and tails heavier than that of a Gaussian PDF, i.e., a heavy-tailed PDF. In this section, the alpha-stable statistical model is used to characterize the contourlet image coefficients. This model is suitable for describing signals with non-Gaussian statistics and heavy tails [48]–[50]. The alpha-stable model requires four parameters for its complete description: a characteristic exponent α, $(0 < \alpha \leq 2)$, a skewness parameter $\beta \in [-1, 1]$, a location parameter $\delta \in \Re$, and dispersion parameter $\gamma > 0$. For one class of the alpha-stable distributions, called the symmetric alpha-stable (SαS) distribution, $\beta = 0$. The univariate zero-mean SαS distribution with a random variable $X \sim \text{S}\alpha\text{S}(\alpha,\gamma)$ is described by its characteristic function

$$\Phi_{\alpha,\gamma}(\omega) = \exp\left(-\gamma\ |\omega|^{\alpha}\right) \tag{1}$$

The dispersion parameter γ determines the spread of the distribution around its location parameter δ, just as the variance

TABLE I
CHARACTERISTIC EXPONENT OF THE ALPHA-STABLE DISTRIBUTION, ESTIMATED FROM DIFFERENT CONTOURLET SUBBAND COEFFICIENTS

Direction	Scale	Barbara	Peppers	Lena	Baboon	Airplane
1	II	1.137	1.330	1.270	1.451	0.973
2		1.135	1.253	1.100	1.445	0.938
3		1.080	1.270	1.090	1.278	0.877
4		1.206	1.317	1.151	1.255	1.040
1	I	0.964	1.432	1.316	1.341	0.994
2		1.024	1.336	1.265	1.467	0.903
3		0.848	1.196	1.216	1.312	0.873
4		1.102	1.216	1.037	1.523	0.902
5		1.375	1.225	1.059	1.412	1.033
6		1.264	1.217	1.170	1.332	1.137
7		1.209	1.115	1.177	1.314	1.094
8		1.591	1.388	1.240	1.425	1.231

is around the mean in the case of the Gaussian distribution. The characteristic exponent α is the most important parameter which determines the shape of the distribution. The smaller the value of α, the heavier the tail of the distribution. This implies that random variables following the SαS distribution with small characteristic exponents are highly impulsive. It should be noted that there is no closed-form expression for the SαS distribution except when $\alpha = 1$ and $\alpha = 2$, which define the Cauchy and the Gaussian processes, respectively. Although the SαS density behaves approximately like a Gaussian density near the origin, its tail decays at a lower rate [48]. Similar to the univariate SαS distribution, a zero-mean bivariate SαS is characterized by its characteristic function given by

$$\Phi_{\alpha,\gamma}(\omega_1, \omega_2) = \exp\left(-\gamma \left|\sqrt{\omega_1^2 + \omega_2^2}\right|^{\alpha}\right) \quad (2)$$

Equivalently, the bivariate SαS PDF is obtained as

$$f_{\alpha,\gamma}(x_1, x_2) = \frac{1}{4\pi^2}\int_{-\infty}^{\infty}\int_{-\infty}^{\infty} e^{\left(j\gamma\left|\sqrt{\omega_1^2+\omega_2^2}\right|^{\alpha}(\omega_1 x_1+\omega_2 x_2)\right)} d\omega_1 d\omega_2. \quad (3)$$

C. Modeling of Contourlet Coefficients Using Univariate SαS

The symmetric alpha-stable family of distributions has attracted attention in the modeling of heavy-tailed data such as the transform-domain image coefficients [7], [51]. In order to model the contourlet subband coefficients of an image, we propose the use of *SαS* distribution. To this end, we estimate the values of the characteristic exponent, α, for the various contourlet subbands when the given test image is decomposed into two pyramidal levels, with eight and four directions, respectively. In Table I, the results obtained by estimating α using the maximum likelihood approach [52], [53] for a few of test images are summarized. It can be seen from this table that the value of α varies from 0.8 to 1.6 indicating the heavy-tailed property of the contourlet coefficients and that the distribution is not Gaussian. Thus, the distribution of the contourlet coefficients of an image can be described by a SαS PDF. We then examine the histograms of the actual data as well as the SαS, Cauchy, GG and the Laplacian density functions for a number

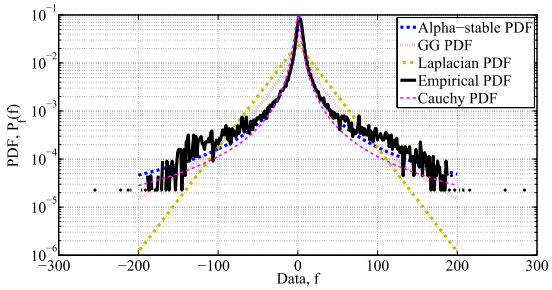

(a)

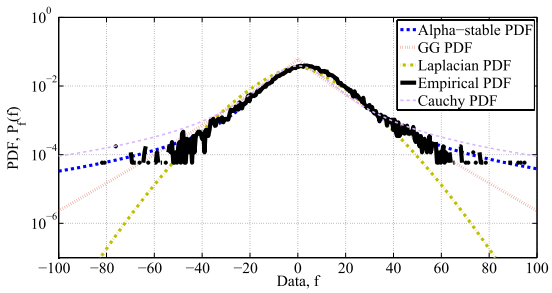

(b)

Fig. 1. The log-scale PDFs of empirical data as well as the SαS, Cauchy, GG and Laplacian distributions for two of the test images (a) *Barbara* $\alpha = 0.8$, (b) *Baboon* $\alpha = 1.31$.

of test images. Moreover, since in the range of α, the alpha-stable PDF does not have a closed form expression except when $\alpha = 1$, corresponding to the Cauchy distribution, we also investigate as to how accurately the Cauchy distribution fits the distribution of the contourlet coefficients. The modeling performance of the contourlet coefficients for two of the images, *Barbara* and *Baboon*, are shown in Fig. 1. It is evident from this figure that the univariate SαS distribution and its Cauchy member for which the empirical data than the GG and Laplacian distributions can. Similar results have also obtained for other test images. Moreover, to quantify the performance of the PDFs, we employ the Kolmogorov-Smirnov distance (KSD) given by $max|\int P_f(f) - \hat{P}_f(f)df|$ in which, $P_f(f)$ denotes the PDF of the random variable and $\hat{P}_f(f)$ represents the PDF of the empirical data. Table II gives the values of the KSD metric for the SαS, Cauchy and GG PDFs of the image contourlet coefficients in two finest scales. These values are obtained by averaging over 96 images. It is seen from this table that the univariate SαS distribution, and its Cauchy member, provide better fits to the empirical data than the GG distribution does. The amplitude probability density (APD) function, given by $P(|X| > x)$, is another common statistical representation of heavy-tailed signals. The APD can be used to compare the closeness of the alpha-stable and Cauchy distributions to the empirical data. It can be empirically calculated by counting the data, X for which $|X| > x$. It can be also evaluated theoretically from a given density function by estimating its parameters from the transformed coefficients. It is known that the alpha-stable density function has a polynomial tail $P(X > x) \sim c_\alpha x^{-\alpha}\gamma^{\alpha}$, $x \to \infty$, where X is a non-Gaussian SαS random variable and $c_\alpha = \sin(\frac{\pi\alpha}{2})\frac{\Gamma(\alpha)}{\pi}$ [43]. We now examine the APD curves of the actual data as well as the SαS, Cauchy, GG and Laplacian distributions for a number

TABLE II
THE AVERAGED KSD VALUES OF THE SαS, CAUCHY AND GG DISTRIBUTIONS IN MODELING OF THE CONTOURLET COEFFICIENTS OVER 96 IMAGES

Direction	Scale	KSD SαS	KSD Cauchy	KSD GG
1	II	0.0353	0.0391	0.0419
2		0.0530	0.0758	0.0790
3		0.0585	0.0593	0.0605
4		0.0541	0.0580	0.0616
1	I	0.0634	0.0896	0.0983
2		0.0642	0.0788	0.0914
3		0.0693	0.0875	0.0993
4		0.0738	0.0901	0.0965
5		0.0754	0.0953	0.1011
6		0.0673	0.0874	0.0964
7		0.0562	0.0734	0.0845
8		0.0634	0.0850	0.0953

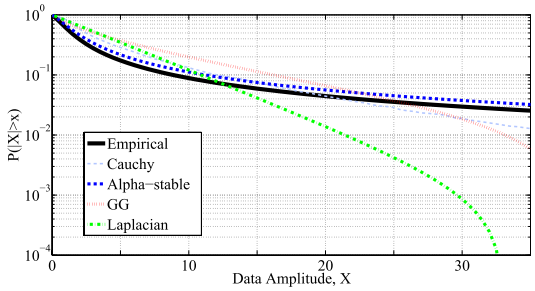

(a)

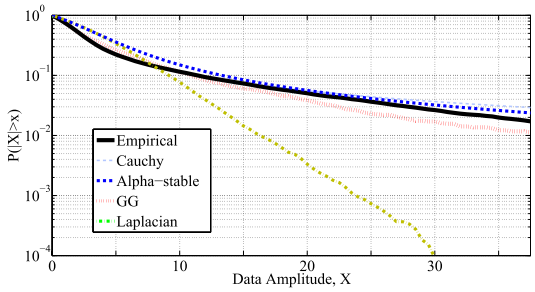

(b)

Fig. 2. APD curves of the empirical data as well as the SαS, Cauchy, GG and Laplacian distributions for two of the test images (a) *Barbara* (b) *Baboon*.

of test images. In Fig. 2, the APD curves for two of the images, *Barbara* and *Baboon*, are depicted. It is seen from this figure that the SαS distribution, and its Cauchy member, provide better fits to the distribution of the contourlet coefficients for both the mode and the tail of the actual data than that provided by the GG and Laplacian distributions. Similar results have also been obtained for other test images.

D. Modeling of Contourlet Coefficients Using Bivariate SαS

It is known that the contourlet coefficients of an image have across scale dependencies with their parents and children [35]. Fig. 3 depicts a parent-children relationship for a three-scale contourlet decomposition with eight directions in each scale. This dependency plays an important role in the modeling of the contourlet coefficients. It is also known that the contourlet coefficients of an image are non-Gaussian [33], [39], i.e., their distributions have large peaks around zero and tails heavier

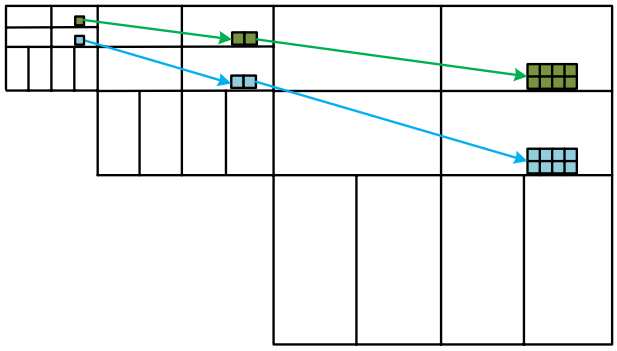

Fig. 3. Parent-children relationship for a three-scale contourlet decomposition with eight directions in each scale.

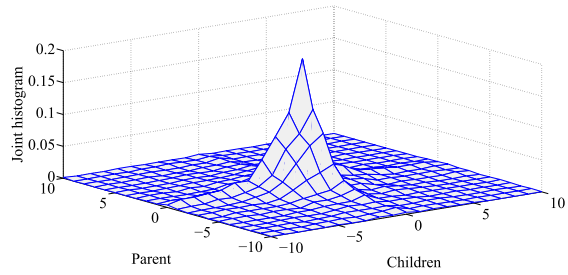

(a)

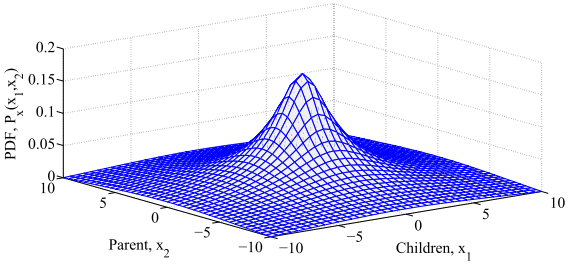

(b)

Fig. 4. The empirical joint child-parent histogram across two scales of the contourlet coefficients for the fourth direction of the *Barbara* image. (b) The configuration of the bivariate SαS distribution.

than that of a Gaussian PDF. In view of this, we also model the contourlet coefficients of an image using the bivariate alpha-stable distribution not only to capture the heavy tails of the distribution of the contourlet coefficients, but also to take into account the contourlet coefficient dependencies across scales. Fig. 4 shows the joint histogram of the contourlet coefficients across scales for one of the test images, *Barbara*, along with a possible configuration of the bivariate SαS PDF. It can be seen from this figure that the bivariate SαS PDF can suitably model the parent-children relationship of the contourlet coefficients across two consecutive scales.

III. WATERMARKING

A. Watermark Embedding

In the embedding process, we focus specifically on a multiplicative spread spectrum scheme, for reasons mentioned in Section I, in the contourlet domain. The contourlet transform is first applied to an image to capture the important features of the image in a few coefficients. It has been shown that a

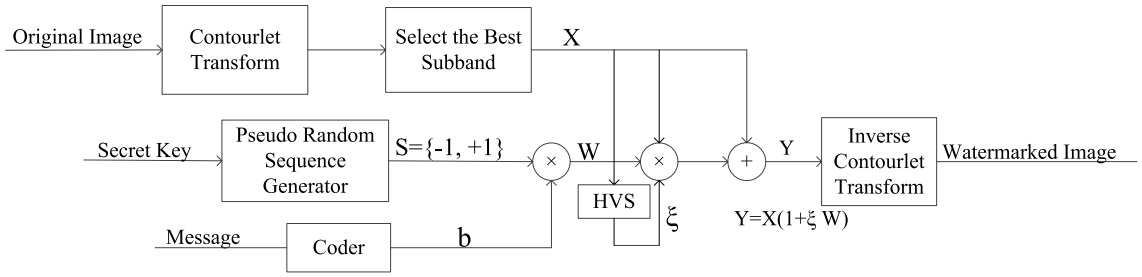

Fig. 5. Block diagram of the watermark embedding procedure; a multiplicative approach is considered.

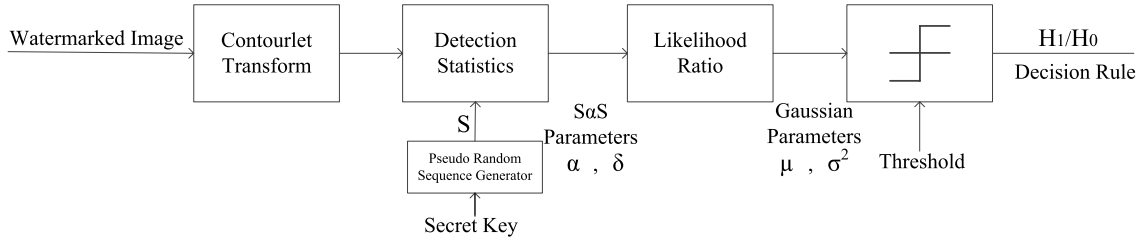

Fig. 6. Block diagram of the watermark detection procedure; a Bayesian log-likelihood ratio is employed.

watermark should be inserted into the significant features of an image in order to increase the robustness of the watermark [3]. In view of this, we are going to find the coefficients that represent most of the features of an image; hence, we compute the energy of the coefficients in each directional subband and then select the subband X that has the highest value for its energy for embedding the watermark. For an $M_1 \times M_2$ image, this subband X is given by

$$\left\{ X = arg \underbrace{max}_{j,d} \left(\sum_{k=1}^{N_j} [C_{j,d}^k]^2 \right) \right\}, \quad N_j = \frac{M_1 M_2}{2^{2(j-1)} D_j} \tag{4}$$

where $j = 1, \ldots, J$ refers to the number of resolution levels and $d = 1, \ldots, D_j$ to the number of frequency directions. Fig. 5 shows a block diagram of the proposed watermark embedding procedure. The watermark sequence W modifies the contourlet coefficients of the selected subband X giving the watermarked coefficients Y. The watermark may or may not contain a message. When the watermark carries a message, the message is coded into a binary sequence $\{b_i\}_{i=1}^N$ with $+1$ for bit 1 and -1 for bit 0 for the message, otherwise $b = 1$, i.e., single bit watermarking. The watermark is generated using a direct sequence spread spectrum technique, wherein the watermark is generated using a pseudorandom sequence generator that has an authentication key as its initial value. This pseudorandom sequence spreads the spectrum of the watermark signal over many coefficients making it difficult to be detected. To maximize the security and robustness of the watermarking scheme, the sequence should have white-noise like properties [7], [15]. Let such a sequence be denoted by $\{s_i\}_{i=1}^N$, where s_i takes the values 1 or -1 with equal probability. In order to assure a robust watermarking scheme, the watermark should have maximum strength without affecting the perceptual quality of the image. For this purpose, a positive watermark weighing factor ζ is used to provide a trade-off between the robustness of the watermarking method and the imperceptibility of the embedded image based on the local characteristics of the image for a given resolution level and frequency direction. The contourlet coefficients of the selected subband are modified as

$$y_i = x_i + \zeta x_i w_i \tag{5}$$

where $\{x_i\}_{i=1}^N$ and $\{y_i\}_{i=1}^N$ are the original and watermarked coefficients, respectively, and $W = \{w_i = b_i s_i\}_{i=1}^N$. The weighting factor ζ is calculated for an image by using the watermark to document ratio (WDR) given by [7], [14], and [15]

$$WDR = 10log \left(\frac{\zeta^2}{\sigma_{x_i}^2} \right) \tag{6}$$

where the term "document" refers to the contourlet coefficients of the original image and $\sigma_{x_i}^2 = \frac{1}{N} \sum_i x_i^2$. In this case, the watermark can be adapted to the local properties of the original image. It should be mentioned that ζ can be increased to a point where the watermark is still invisible, and yet it is still detectable. The watermarked contourlet coefficients are then inverse transformed to obtain the watermarked image.

B. Watermark Detection

In general, a watermarking scheme for copyright protection has an embedded watermark that is known to the intended receiver. Hence, the verification of its existence, i.e., the detection of the watermark, is sufficient for the purpose of checking the authenticity of the copyright. Fig. 6 gives a block diagram of the different steps involved in the watermark verification process. Current detection methods use the signal statistics for the watermark detection [6]–[12], [15]–[19]. In this work, we employ a Bayesian log-likelihood ratio test for detecting the watermark in the contourlet coefficients of a watermarked image. This method can be reduced to a binary hypothesis test to verify the presence of a watermark. It consists of testing an *alternative hypothesis* H_1 against a *null hypothesis* H_0 and can be mathematically formulated based on the statistical properties of the contourlet coefficients [34]. The hypotheses

H_1 and H_0 represent as to whether the contourlet coefficients are watermarked by the sequence W or do not carry any watermark, respectively, and can be stated as

$$\begin{aligned} H_1 &: Y = X + \zeta XW \\ H_0 &: Y = X \end{aligned} \tag{7}$$

In detection, the goal is to see whether or not there is a watermark in the received image Y, based on the statistical properties of the original image X. The data is modeled by an appropriate statistical distribution by assuming independence of the observations. The decision rule is then defined as the likelihood ratio $\Lambda_{det}(Y)$

$$\Lambda_{det}(Y) = \frac{f_y(Y|H_1)}{f_y(Y|H_0)} \tag{8}$$

which is then compared to the detection threshold τ

$$\Lambda_{det} \underset{H_0}{\overset{H_1}{\gtrless}} \tau \tag{9}$$

The likelihood ratio uses the PDFs under each hypothesis as

$$\begin{aligned} f_y(Y|H_1) &= \frac{1}{1+\zeta W} f_x\left(\frac{Y}{1+\zeta W}\right) \\ f_y(Y|H_0) &= f_x(Y) \end{aligned} \tag{10}$$

The likelihood ratio becomes

$$\Lambda_{det}(Y) = \prod_{i=1}^{N} \frac{P\left(\frac{y_i}{1+\zeta w_i}\right)}{P(y_i)} \cdot \frac{1}{1+\zeta w_i} \tag{11}$$

In practice, the log-likelihood ratio is usually preferred in hypothesis testing [34], [55], [56] and is defined as the natural logarithm of $\Lambda_{det}(Y)$; hence, the decision rule becomes

$$ln(\Lambda_{det}) \underset{H_0}{\overset{H_1}{\gtrless}} ln(\tau) \tag{12}$$

and the log-likelihood ratio is

$$ln(\Lambda_{det}(Y)) = \sum_{i=1}^{N} ln\left(\frac{P\left(\frac{y_i}{1+\zeta w_i}\right)}{P(y_i)} \cdot \frac{1}{1+\zeta w_i}\right) \tag{13}$$

The detector is supposed to choose between H_1 and H_0 based on the received image Y. In this case, if $ln(\Lambda_{det}(Y)) > \tau$, H_1 is accepted; otherwise, H_0 is accepted. The log-likelihood ratio is clearly a superposition of N statistically independent random variables with finite mean and variance. Thus, according to the central limit theorem for large N [55], the log-likelihood ratio follows an approximately Gaussian distribution under each hypothesis. The mean and variance of each of the Gaussian distributions can be estimated from the empirical data and are given by (μ_0, σ_0^2) and (μ_1, σ_1^2), for H_0 and H_1, respectively. It is known that in the decision task there may be two types of errors [56]. Type I error occurs when detector decides H_1 when in fact H_0 is correct. This error is called the probability of false-alarm denoted by P_{fa}. Type II error occurs when H_0 is accepted while H_1 is correct.

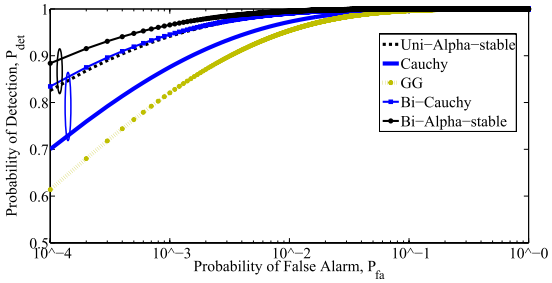

Fig. 7. ROC curves for the univariate and bivariate SαS, univariate and bivariate Cauchy and GG distributions obtained by averaging on 96 images.

This error is called miss-detection denoted by $P_m = 1 - P_{det}$, where P_{det} is the detection probability of accepting H_1 when the watermark is present. Since, there is no closed-form expression for the SαS distribution except when α takes the values 1 for the Cauchy or 2 for the Gaussian distributions, in order to design the watermark detector i.e., finding the mean and variance of the log-likelihood ratio, using the best-fit $S\alpha S$, we resort to a Monte Carlo simulation to numerically find the log-likelihood ratio $ln(\Lambda_{det})$. To this end, 1000 randomly generated watermark sequences that have uniquely-defined keys are employed. For each run, we first estimate the $ln(\Lambda_{det})$ of an image using (13) for both the hypotheses. The experimental mean and variance of $ln(\Lambda_{det})$ are then estimated. Thus, when the mean and variance of the log-likelihood ratio under both hypotheses are known, for a particular value of τ, the probabilities of false alarm and detection can be estimated as [56]

$$\begin{aligned} P_{fa} &= Q\left(\frac{\tau-\mu_0}{\sigma_0}\right) \\ P_{det} &= Q\left(\frac{\tau-\mu_1}{\sigma_1}\right) \end{aligned} \tag{14}$$

where $Q(x)$ is defined as $Q(x) = \frac{1}{\sqrt{2\pi}} \oint_x^\infty e^{-z^2/2} dz$. The decision threshold is obtained by using the Neyman-Pearson criterion that minimizes the probability of miss-detection (i.e., $1 - P_{det}$) for a given probability of false alarm P_{fa} [7], [15] and can be expressed as

$$\tau = \sigma_0 Q^{-1}(P_{fa}) + \mu_0 \tag{15}$$

and P_{det} as

$$P_{det} = Q\left(\frac{\sigma_0}{\sigma_1} Q^{-1}(P_{fa}) - \frac{\mu_1 - \mu_0}{\sigma_1}\right) \tag{16}$$

The performance of the proposed statistical detector can be analyzed theoretically by relating the probability of detection and the probability of false alarm. Resulting curves are called the receiver operating characteristics (ROC). It should be noted that the probability of detection needs to be kept at a high level for a predefined rate of false alarm to increase the reliability of detection. Fig. 7 depicts the corresponding experimental ROC curves for the bivariate and univariate SαS distribution by averaging over 96 images. This figure also shows the theoretical ROC curves for the bivariate and univariate Cauchy with $\alpha = 1$ and GG distributions. The theoretical ROCs can be derived by obtaining the mean and variance of the log-likelihood ratio under each hypothesis. Using the

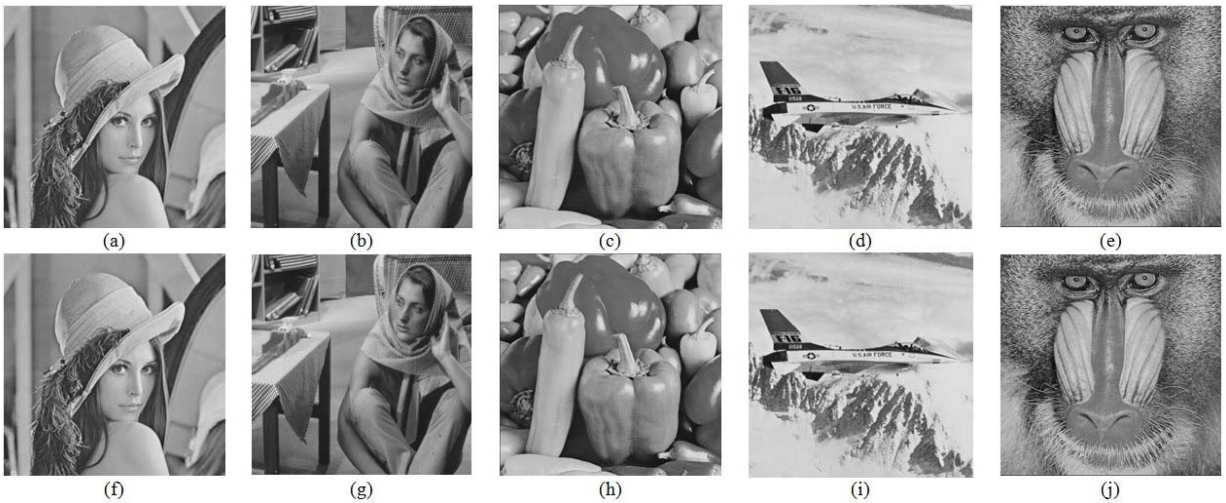

Fig. 8. Original (a-e) and watermarked with $WDR = -40$ dB (f-j) images of *Lena* PSNR = 58.42, *Barbara* PSNR = 52.19, *Peppers* PSNR = 60.20, *Airplane* PSNR = 56.85 and *Baboon* PSNR = 53.35. No visual difference can be realized.

bivariate Cauchy PDF, given by $f_\gamma(x_1, x_2) = \frac{\gamma}{2\pi(x_1^2+x_2^2+\gamma^2)^{3/2}}$, the theoretical mean and variance of $ln(\Lambda_{det})$ under H_0 (note that $y_i = x_i$) can be shown to be (see the Appendix)

$$\begin{aligned}\mu_0 &= E[ln(\Lambda_{det})|H_0] \\ &= -\frac{ln(1+\zeta)+ln(1-\zeta)}{2} \\ &\quad + \frac{3}{2}\sum_{i=1}^{N} ln\left(\frac{\gamma^2+x_{i1}^2+x_{i2}^2}{((\gamma^2+(\frac{x_{i1}}{1+\zeta})^2+x_{i2}^2)(\gamma^2+(\frac{x_{i1}}{1-\zeta})^2)+x_{i2}^2)^{1/2}}\right)\end{aligned} \tag{17}$$

and

$$\begin{aligned}\sigma_0^2 &= VAR[ln(\Lambda_{det})|H_0] \\ &= E\left[ln(\Lambda_{det}) - E[ln(\Lambda_{det})|H_0]\right]^2 \\ &= \sum_{i=1}^{N}\frac{1}{4}\left(ln\frac{1+\zeta}{1-\zeta} + ln\frac{\gamma^2+(\frac{x_{i1}}{1-\zeta})^2+x_{i2}^2}{\gamma^2+(\frac{x_{i1}}{1+\zeta})^2+x_{i2}^2}\right)^2\end{aligned} \tag{18}$$

where parameter γ of the bivariate Cauchy distribution can be directly computed from the children contourlet coefficients of the watermarked image. To obtain the mean and variance of the log-likelihood ratio, following assumptions have been made. 1) The number of directions in each scale should be the same in order to have a relation between the parents and their children in each direction. 2) The watermark is embedded only in the children subband. To have both x_{i1} and x_{i2} to be of the same size, we expand the parent subband by a factor of 2.

It should be noted that the PDF of the original and watermarked images are assumed to be the same, i.e., embedding the watermark does not change the distribution of the original image coefficients [7], [8]. The mean and variance of the log-likelihood ratio under H_1 can also be found in a similar manner. It can easily be shown that $\mu_0 = -\mu_1$ and $\sigma_0^2 = \sigma_1^2$. It is seen from Fig. 7 that the detectors based on the bivariate SαS distribution, and even its Cauchy member, have higher rates of detection for a given probability of false alarm than that based on the GG distribution. We also obtain the CPU times for the detectors based on these distributions; Table III gives the CPU times averaged over 96 images. It is observed from this table that the CPU time when using the best-fit bivariate and univariate SαS is indeed high. Thus, the slight performance improvement of the bivariate SαS over that using bivariate Cauchy distribution, as seen from Fig. 7, is at the expense of a substantially high computational complexity. Therefore, without any appreciable loss of the rate of detection, a watermark detector is also designed based on the bivariate Cauchy distribution. It should be noted that the bivariate Cauchy distribution has a closed form expression for its PDF which leads to a computationally efficient detector with low CPU time required.

IV. Experimental Results

Experiments are conducted to investigate the imperceptibility of the embedded watermark as well as the robustness of the proposed method against attacks. The standard images considered in these experiments are 96 images, each of size 512×512 [57] and are implemented in MATLAB on an Intel Core *i*7 2.93 GHz personal computer with 8 GB RAM. However, the results for a few of the images are included in the paper due to space limitations. In our experiments, the watermark is generated following the procedure described in Section IV (a). To select the appropriate subband for embedding the watermark bits adopting the multiplicative embedding rule, both the robustness and the visual quality of watermarked image should be considered. In view of this, we embed the watermark through the following procedure:

1) Decompose the original image into a number of subbands by using the contourlet transform with two pyramidal levels followed by eight directions in each scale.
2) Compute the energy of each subband by using (2) and choosing the subband that has the highest energy for embedding the watermark.
3) By using (3), we can embed the watermark in a multiplicative manner.
4) Apply the inverse contourlet transform to the modified coefficients to obtain the watermarked image.

In Fig. 8(a)-(e), a few of the original images namely, *Lena*, *Barbara*, *Peppers*, *Airplane* and *Baboon* are presented and the

TABLE III
THE AVERAGED CPU TIMES OF THE DETECTORS USING THE BIVARIATE AND UNIVARIATE SαS, BIVARIATE AND UNIVARIATE CAUCHY AND GG DISTRIBUTIONS

	bi-SαS	SαS	bi-Cauchy	Cauchy	GG
CPU time (sec)	63.50	43.47	3.12	1.85	1.84

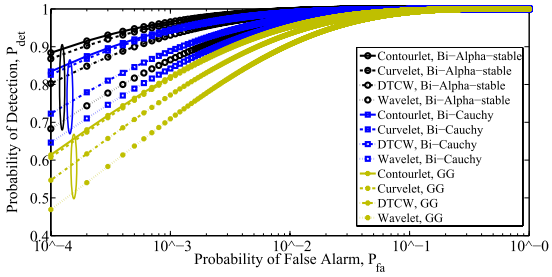

Fig. 9. ROC curves for contourlet, curvelet, wavelet and dual-tree complex wavelet (DTCW) transforms obtained by averaging on 96 images.

watermarked images with $WDR = -40$ dB in Fig. 8(f)-(j). The images are indistinguishable with high PSNR values, thus showing the effectiveness of the multiplicative contourlet-domain watermarking in terms of the invisibility of the watermark. Watermark detection is performed without requiring the use of the original image (i.e., blind image watermarking). In order to compare the performance of the contourlet transform with other sparse transforms such as wavelet, dual-tree complex wavelet and curvelet transforms, we consider two-level decomposition for each transform and a same-size watermark inserted in their subband coefficients. The ROC curves for various transforms are derived for the univariate Cauchy and GG distributions. Fig. 9 depicts the ROC curves obtained for one of the test images, the *Barbara* image. It is seen from this figure that the contourlet and curvelet transforms have the best rates of detection as compared to the other transforms. Similar results are obtained for other test images. The reason for better rates of detection for these two transforms is due to their capability in capturing more geometrical shapes by allowing for a flexible number of directions at each scale [39], [40]. However, the fact that the contourlet transform has been defined directly in the discrete domain along with its 2D frequency partitioning on concentric rectangles rather than on concentric circles for curvelet, has motivated us to use the contourlet transform in our work. Table IV gives the CPU times averaged over 96 images, required by the detectors using the contourlet and curvelet transforms. It is seen from this table that the detector using the contourlet transform has a very much lower computational complexity compared to that using the curvelet transform. The significantly lower CPU time for the contourlet-based method can be attributed to the fact that this transform is not only defined directly in the discrete domain, but also employs iterated filter banks making it computationally efficient.

Now, for each image, the performance of the bivariate Cauchy detector is first compared to that of the GG detector in terms of the ROC curves without any kind of attack. It is to be pointed out that the theoretical ROC can be computed

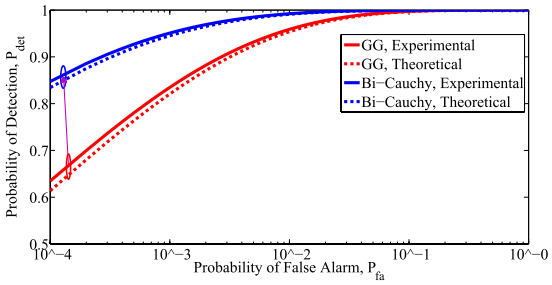

Fig. 10. Theoretical and experimental ROC curves for the bivariate Cauchy and GG detectors obtained by averaging on 96 images.

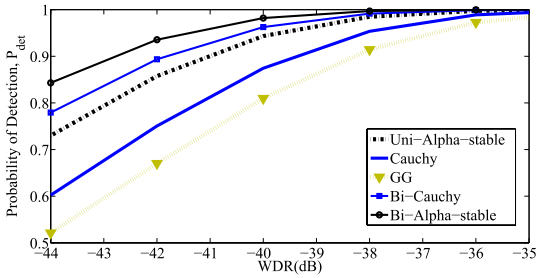

Fig. 11. Probability of detection for watermarks of varying strength parametrized by the WDR(dB) for various detectors obtained by averaging on 96 images.

TABLE IV
THE AVERAGED CPU TIMES OF THE UNIVARIATE CAUCHY DETECTOR USING THE CONTORLET AND CURVELET TRANSFORMS

	Contourlet	Curvelet
CPU time (sec)	1.85	213.90

directly from the data by estimating the parameters for each of the two distributions. To validate this theoretical ROC, Monte Carlo simulations are performed. The experimental mean and variance of $ln(\Lambda_{det})$ for each of the detectors are estimated. The theoretical and experimental ROC curves averaged over 96 images are shown in Fig. 10 for the bivariate Cauchy and GG detectors. It is seen from this figure that the experimental ROC curves are very close to the theoretical ones for both the detectors. It is also seen that the bivariate Cauchy detector yields a performance which is much better than that of the GG detector as evidenced by a higher probability of detection for any given value of false alarm.

In order to compare the performance of the detectors for watermarks with different strengths, we consider WDR in the range -42 dB to -32 dB for all the test images. Fig. 11 shows the results of detection rate averaged over 96 images when P_{fa} is fixed at 10^{-3}. From this figure, it can be seen that as WDR decreases, the performances of all the detectors deteriorate. However, the bivariate SαS and bivariate Cauchy detectors outperform the GG detector at any level of the watermark strength, as can be seen from the values of the detection probabilities.

Fig. 12 shows that the probability of false alarm, P_{fa}, as a function of the strength of the watermark, WDR, for a fixed value of the probability of detection $P_{det} = 0.9$. It is seen from this figure that the probability of false alarm for the proposed bivariate SαS and bivariate Cauchy detectors are lower than

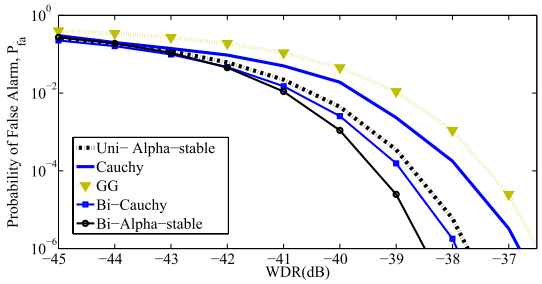

Fig. 12. Probability of false alarm for watermarks of varying strength parametrized by WDR(dB) for various detectors obtained by averaging on 96 images.

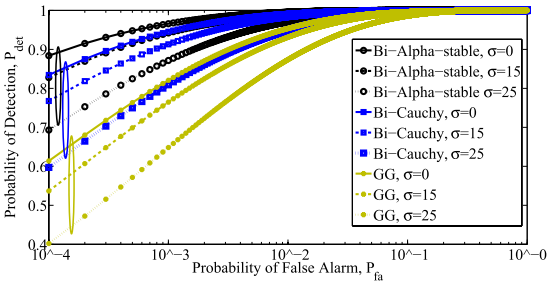

Fig. 13. ROC curves obtained by averaging on 96 images for various detectors when the AWGN with various standard deviations is added to the watermarked images.

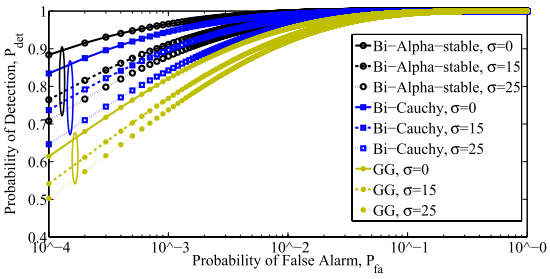

Fig. 14. ROC curves obtained by averaging on 96 images for various detectors when images are under salt & pepper noise.

that of the GG detector for different watermark strengths. The robustness of the detectors against various attacks is next studied using the same set of images. To study the robustness against noise, the watermarked images are first corrupted by AWGN with σ varying from 0 to 25. Fig. 13 shows the averaged ROC curves obtained using various detectors when the watermarked image is contaminated by AWGN noise. It is seen from this figure that the proposed bivariate SαS and bivariate Cauchy detectors are more robust than the GG detector is. The performance against the salt & pepper noise attack is also tested when σ of the noise is varied from 0 to 25. Fig. 14 shows the averaged ROC curves for various detectors. It is seen from this figure that the proposed watermarking algorithm using the bivariate SαS and bivariate Cauchy detectors are more robust against salt & pepper noise also. The robustness of the proposed detector under JPEG compression is now investigated. For this purpose, we compare the log-likelihood ratio, $ln(\Lambda_{det})$, with the decision threshold τ for a given false alarm probability to obtain the detector response for a given image. The detector responses of the proposed watermarking scheme with the bivariate SαS and bivariate and univariate Cauchy detectors as well as that with the GG

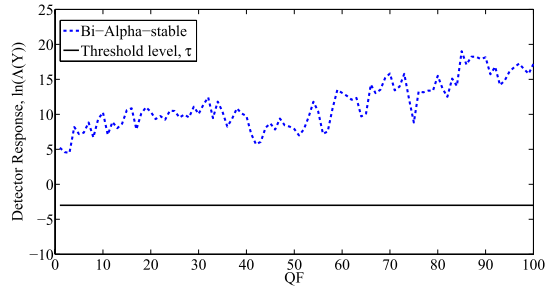

(a)

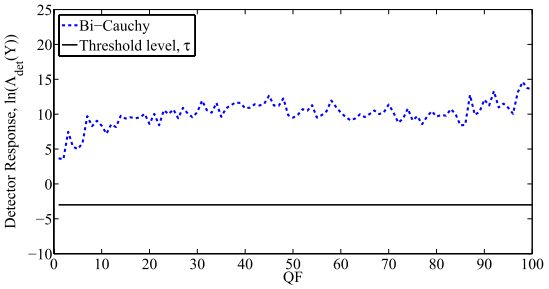

(b)

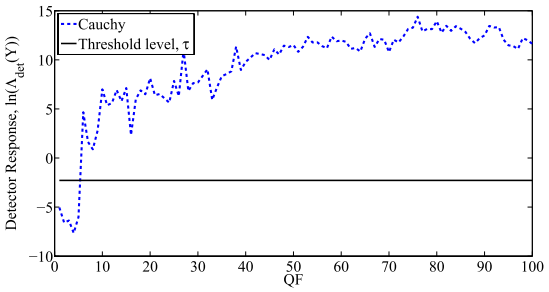

(c)

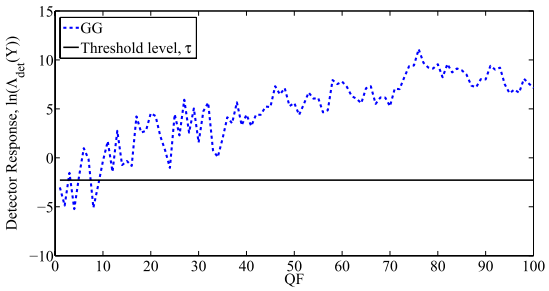

(d)

Fig. 15. Detector response for the (a) bivariate alpha-stable, (b) bivariate Cauchy, (c) univariate Cauchy and (d) GG distributions when the *Lena* image is JPEG-compressed with different quality factors varying from 1 to 100, WDR $= -38$ dB.

detector for one of the test images, the *Lena* image, are shown in Fig. 15. It is seen from this figure that by using the proposed watermarking scheme with the bivariate SαS detector and even its Cauchy member, a higher detection rate is obtained and that the scheme is more robust than the one with the GG detector. Finally, the robustness of the proposed scheme when the watermarked image undergoes median filtering is studied. Fig. 16 shows the detector responses of the proposed watermarking scheme with the bivariate SαS and bivariate and univariate Cauchy detectors as well as that with the GG detector for the *Lena* image with windows of size 3×3, 5×5

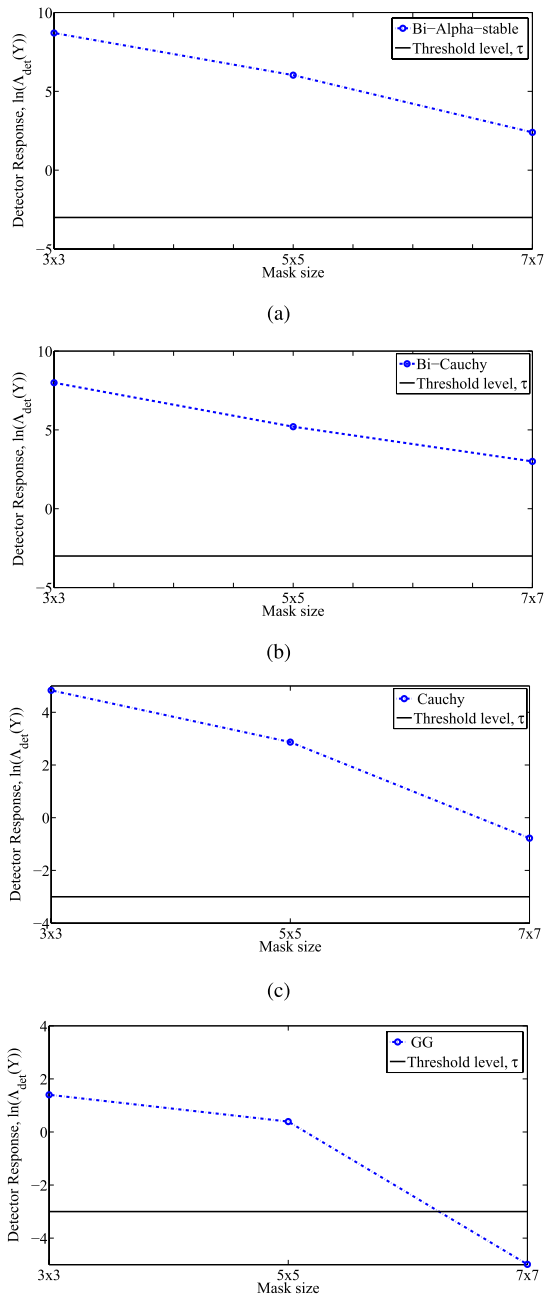

Fig. 16. Detector response for the (a) bivariate alpha-stable, (b) bivariate Cauchy, (c) univariate Cauchy and (d) GG distributions when the *Lena* image is under median filtering with windows of size of 3×3, 5×5 and 7×7; WDR $= -38$ dB.

and 7×7 for the median filter. It is evident from this figure that for the window size of 7×7, the GG detector cannot even recognize the presence of the watermark. Thus, the proposed scheme using the bivariate SαS and bivariate Cauchy detectors are much more robust than that with the GG detector.

V. Conclusion

In this paper, we have first studied the suitability of the univariate and bivariate alpha-stable distributions in modeling the contourlet coefficients of an image. We have shown that the univariate alpha-stable distribution provides a more accurate fit to the empirical data in terms of the Kolmogorov-Smirnov distance as well as through a visual comparison of the histograms of various distributions. We have also shown that the bivariate alpha-stable distribution can capture the across-scale dependencies between the contourlet coefficients. Motivated by these modeling results, blind watermark detectors in the contourlet domain using both the univariate and bivariate alpha-stable distributions have been designed. The proposed detectors employ the Bayesian log-likelihood ratio criterion for the watermark detection. It has been shown that the detectors based on both of these distributions have higher rates of detection for a given probability of false alarm than that based on the GG distribution has. Even though the detector based on the general alpha-stable distribution (with the best-fit alpha) provides a higher detection rate, it is computationally expensive because of the lack of a closed form expression for its distribution. In view of this, a watermark detector has been designed based on the bivariate Cauchy member of the alpha-stable family. It has been shown that a very significant advantage of the closed-form expression of the bivariate Cauchy PDF is that it allows a derivation of closed-form expressions for the mean and variance of the log-likelihood ratio in terms of the empirical data. This has resulted in the design of a significantly reduced-complexity detector, yet providing a performance that is much superior to that of the GG detector and very close to that corresponding to the best-fit alpha detector. The performance of the proposed detectors have been evaluated in detail by conducting several experiments. The robustness of the proposed detectors, using the bivariate alpha-stable and bivariate Cauchy PDFs, against additive white Gaussian noise, salt & pepper noise, JPEG compression and median filtering attacks has been studied and shown to be superior to that of the GG detector.

Appendix

Mean and Variance of the Log-Likelihood Ratio Under the Hypothesis H_0 for the Bivariate Cauchy Distribution

For the multiplicative watermarking scheme given by (5), the likelihood ratio $\Lambda_{det}(Y)$ is obtained as

$$\Lambda_{det}(Y) = \sum_{i=1}^{N} \frac{P(\frac{y_i}{1+\zeta w_i})}{P(y_i)} \cdot \frac{1}{1+\zeta w_i} \tag{A.1}$$

Therefore, the log-likelihood ratio is given by

$$ln(\Lambda_{det}(Y)) = \sum_{i=1}^{N} ln\left(\frac{P(\frac{y_i}{1+\zeta w_i})}{P(y_i)} \cdot \frac{1}{1+\zeta w_i}\right) \tag{A.2}$$

which for the bivariate Cauchy distribution can be written as

$$ln(\Lambda_{det}(Y)) = \frac{3}{2}\sum_{i=1}^{N} ln\left(\frac{\gamma^2 + y_{i1}^2 + y_{i2}^2}{\gamma^2 + (\frac{y_{i1}}{1+\zeta w_i})^2 + y_{i2}^2}\right) + \sum_{i=1}^{N} ln\left|\frac{1}{1+\zeta w_i}\right| \tag{A.3}$$

Let $ln(\Lambda_{det}(Y)) = q_1(Y) + \frac{3}{2}q_2(Y)$ where

$$q_1(Y) = -ln(1+\zeta W)$$
$$q_2(Y) = ln\left(\frac{\gamma^2 + Y_1^2 + Y_2^2}{\gamma^2 + (\frac{Y_1}{1+\zeta W})^2 + Y_2^2}\right) \quad \text{(A.4)}$$

It is known in that for large N, the log-likelihood ratio under both the hypotheses can be approximated by Gaussian distributions with means (μ_0, μ_1) and variances (σ_0^2, σ_1^2) [55]. The mean and variance of the log-likelihood ratio under H_0 (i.e., $y_i = x_i$) can be obtained as [33], [50]

$$\mu_0 = \mu(ln(\Lambda_{det}(Y)); H_0) = \sum_{i=1}^{N}\left(\mu_{q_1} + \mu_{q_2}\right) \quad \text{(A.5)}$$

and

$$\sigma_0^2 = \sigma^2(ln(\Lambda_{det}(Y)); H_0)$$
$$= \sum_{i=1}^{N}\left(\sigma_{q_1}^2 + \sigma_{q_2}^2 - 2\mu_{q_1q_2} + 2\mu_{q_1}\mu_{q_2}\right) \quad \text{(A.6)}$$

In Section III (A), we assumed that the watermark sequence W is generated by a pseudorandom sequence taking values $+1$ and -1 with equal probability. Hence, μ_{q_1} and μ_{q_2} can be obtained as

$$\mu_{q_1} = -\frac{1}{2}\left(ln(1+\zeta) + ln(1-\zeta)\right) \quad \text{(A.7)}$$

and

$$\mu_{q_2} = ln\left(\gamma^2 + X_1^2 + X_2^2\right) - \frac{1}{2}ln\left(\gamma^2 + (\frac{X_1}{1+\zeta})^2 + X_2^2\right)$$
$$-\frac{1}{2}ln\left(\gamma^2 + (\frac{X_1}{1-\zeta})^2 + X_2^2\right) \quad \text{(A.8)}$$

And hence μ_0 can be calculated using (A.5). In order to find the variance of the log-likelihood ratio, given by (A.6), the various terms are found and given below

$$\sigma_{q_1}^2 = E[q_1^2] - \mu_{q_1} = \frac{1}{4}\left(ln(1+\zeta) + ln(1-\zeta)\right)^2 \quad \text{(A.9)}$$

$$\sigma_{q_2}^2 = E[q_2^2] - \mu_{q_2} = \frac{1}{4}\left(ln\frac{\gamma^2 + (\frac{X_1}{1-\zeta})^2 + X_2^2}{\gamma^2 + (\frac{X_1}{1+\zeta})^2 + X_2^2}\right)^2 \quad \text{(A.10)}$$

$$\mu_{q_1q_2} = -\frac{1}{2}\left(ln(1+\zeta)\frac{\gamma^2 + X_1^2 + X_2^2}{\gamma^2 + (\frac{X_1}{1+\zeta})^2 + X_2^2}\right)$$
$$-\frac{1}{2}\left(ln(1-\zeta)\frac{\gamma^2 + X_1^2 + X_2^2}{\gamma^2 + (\frac{X_1}{1-\zeta})^2 + X_2^2}\right) \quad \text{(A.11)}$$

and

$$\mu_{q_1}\mu_{q_2} = -\frac{1}{2}\left(ln(1+\zeta) + ln(1-\zeta)\right)$$
$$\cdot\left[ln\frac{\gamma^2 + X_1^2 + X_2^2}{\left((\gamma^2 + (\frac{X_1}{1+\zeta})^2 + X_2^2)(\gamma^2 + (\frac{X_1}{1-\zeta})^2 + X_2^2)\right)^{1/2}}\right] \quad \text{(A.12)}$$

Then, after some mathematical manipulations, the final expression for the variance, as given by (18), can be obtained. In a similar manner, the mean and variance of the log-likelihood ratio under H_0 for the GG distribution with the PDF given by $f_{X,GG}(x) = \frac{c}{2a\Gamma(1/c)}\exp\left(-\left|\frac{x-\mu}{a}\right|^c\right)$, where $c > 0$ is a shape parameter, $a > 0$ and μ are the scale parameter and mean of the GG distribution, respectively, can be obtained as

$$\mu_{0,GG} = -\sum_{i=1}^{N}\frac{ln(1+\zeta) + ln(1-\zeta)}{2}$$
$$+\left|\frac{x_i}{2a}\right|^2\left(2 - (1+\zeta)^{-c} - (1-\zeta)^{-c}\right) \quad \text{(A.13)}$$

and

$$\sigma_{0,GG}^2 = \sum_{i=1}^{N}\left|\frac{x_i}{4a^2}\right|^{2c}\left((1-\zeta)^{-c} - (1+\zeta)^{-c}\right)^2$$
$$+\left|\frac{x_i}{a}\right|^c\left((-(ln(1+\zeta))(1-\zeta)^{-c}\right.$$
$$\left.-(ln(1-\zeta))(1+\zeta)^{-c})\right)$$
$$+\frac{(ln(1-\zeta) - ln(1+\zeta))^2}{4} \quad \text{(A.14)}$$

By inserting (A.13) and (A.14) into (13), the ROC curves for the GG detector are derived.

REFERENCES

[1] I. J. Cox, M. L. Miller, and J. A. Bloom, *Digital Watermarking*. San Mateo, CA, USA: Morgan Kaufmann, 2001.

[2] G. C. Langelaar, I. Setyawan, and R. L. Lagendijk, "Watermarking digital image and video data. A state-of-the-art overview," *IEEE Signal Process. Mag.*, vol. 17, no. 5, pp. 20–46, Sep. 2000.

[3] I. J. Cox, J. Kilian, F. T. Leighton, and T. Shamoon, "Secure spread spectrum watermarking for multimedia," *IEEE Trans. Image Process.*, vol. 6, no. 12, pp. 1673–1687, Dec. 1997.

[4] C.-T. Hsu and J.-L. Wu, "Hidden digital watermarks in images," *IEEE Trans. Image Process.*, vol. 8, no. 1, pp. 58–68, Jan. 1999.

[5] I. G. Karybaliand and K. Berberidis, "Efficient spatial image watermarking via new perceptual masking and blind detection schemes," *IEEE Trans. Inf. Forensics Security*, vol. 1, no. 2, pp. 256–274, Jun. 2006.

[6] J. R. Hernández, M. Amado, and F. Pérez-González, "DCT-domain watermarking techniques for still images: Detector performance analysis and a new structure," *IEEE Trans. Image Process.*, vol. 9, no. 1, pp. 55–68, Jan. 2000.

[7] A. Briassouli, P. Tsakalides, and A. Stouraitis, "Hidden messages in heavy-tails: DCT-domain watermark detection using alpha-stable models," *IEEE Trans. Multimedia*, vol. 7, no. 4, pp. 700–715, Aug. 2005.

[8] V. R. Doncel, N. Nikolaidis, and I. Pitas, "An optimal detector structure for the Fourier descriptors domain watermarking of 2D vector graphics," *IEEE Trans. Vis. Comput. Graphics*, vol. 13, no. 5, pp. 851–863, Sep./Oct. 2007.

[9] Q. Cheng and T. S. Huang, "An additive approach to transform-domain information hiding and optimum detection structure," *IEEE Trans. Multimedia*, vol. 3, no. 3, pp. 273–284, Sep. 2001.

[10] A. Nikolaidis and I. Pitas, "Asymptotically optimal detection for additive watermarking in the DCT and DWT domains," *IEEE Trans. Image Process.*, vol. 12, no. 5, pp. 563–571, May 2003.

[11] Q. Cheng and T. S. Huang, "Optimum detection and decoding of multiplicative watermarks in DFT domain," in *Proc. IEEE Int. Conf. Acoust., Speech, Signal Process. (ICASSP)*, May 2002, pp. IV-3477–IV-3480.

[12] Q. Cheng and T. S. Huang, "Robust optimum detection of transform domain multiplicative watermarks," *IEEE Trans. Signal Process.*, vol. 51, no. 4, pp. 906–924, Apr. 2003.

[13] M. Barni, F. Bartolini, and A. Piva, "Improved wavelet-based watermarking through pixel-wise masking," *IEEE Trans. Image Process.*, vol. 10, no. 5, pp. 783–791, May 2001.

[14] A. K. Mairgiotis, N. P. Galatsanos, and Y. Yang, "New additive watermark detectors based on a hierarchical spatially adaptive image model," *IEEE Trans. Inf. Forensics Security*, vol. 3, no. 1, pp. 29–37, Mar. 2008.

[15] S. M. M. Rahman, M. O. Ahmad, and M. N. S. Swamy, "A new statistical detector for DWT-based additive image watermarking using the Gauss–Hermite expansion," *IEEE Trans. Image Process.*, vol. 18, no. 8, pp. 1782–1796, Aug. 2009.

[16] Q. Cheng and T. S. Huang, "Optimum detection of multiplicative watermarks using locally optimum decision rule," in *Proc. IEEE Int. Conf. Multimedia Expo*, Aug. 2001, pp. 309–312.

[17] M. Barni, F. Bartolini, A. de Rosa, and A. Piva, "Optimum decoding and detection of multiplicative watermarks," *IEEE Trans. Signal Process.*, vol. 51, no. 4, pp. 1118–1123, Apr. 2003.

[18] J. Zhong and S. Huang, "An enhanced multiplicative spread spectrum watermarking scheme," *IEEE Trans. Circuits Syst. Video Technol.*, vol. 16, no. 12, pp. 1491–1506, Dec. 2006.

[19] M. Barni, F. Bartolini, A. de Rosa, and A. Piva, "A new decoder for the optimum recovery of nonadditive watermarks," *IEEE Trans. Image Process.*, vol. 10, no. 5, pp. 755–766, May 2001.

[20] X. Yin, S. Peng, and X. Zhu, "Detection for multiplicative watermarking in DCT domain by Cauchy model," *Inform. Commun. Security, Lect. Notes Comput. Sci.*, vol. 7043, pp. 173–183, Nov. 2011.

[21] S.-H. Wang and Y.-P. Lin, "Wavelet tree quantization for copyright protection watermarking," *IEEE Trans. Image Process.*, vol. 13, no. 2, pp. 154–165, Feb. 2004.

[22] T. M. Ng and H. K. Garg, "Maximum-likelihood detection in DWT domain image watermarking using Laplacian modeling," *IEEE Signal Process. Lett.*, vol. 12, no. 4, pp. 285–288, Apr. 2005.

[23] B. Chen and G. W. Wornell, "Quantization index modulation: A class of provably good methods for digital watermarking and information embedding," *IEEE Trans. Inf. Theory.*, vol. 47, no. 4, pp. 1423–1443, May 2001.

[24] B. C. Mohan and S. S. Kumar, "Robust digital watermarking scheme using contourlet transform," *Int. J. Comput. Sci. Netw. Security*, vol. 8, no. 2, pp. 43–51, 2008.

[25] A. Giakoumaki, S. Pavlopoulos, and D. Koutsouris, "A medical image watermarking scheme based on wavelet transform," in *Proc. 25th Annu. Int. Conf. IEEE Eng. Med. Biol. Soc.*, Sep. 2003, pp. 856–859.

[26] H. Sadreazami and M. Amini, "A robust spread spectrum based image watermarking in ridgelet domain," *Int. J. Electron. Commun.*, vol. 66, no. 5, pp. 364–371, 2012.

[27] F. Rahimi and H. Rabbani, "A dual adaptive watermarking scheme in contourlet domain for DICOM images," *Biomed. Eng. Online*, vol. 10, p. 53, Jun. 2011.

[28] M. Jayalakshmi, S. N. Merchant, and U. B. Desai, "Digital watermarking in contourlet domain," in *Proc. 18th Int. Conf. Pattern Recognit.*, vol. 3. 2006, pp. 861–864.

[29] H. Song, S. Yu, X. Yang, L. Song, and C. Wang, "Contourlet-based image adaptive watermarking," *Signal Process., Image Commun.*, vol. 23, no. 3, pp. 162–178, 2008.

[30] S. Ghannam and F. E. Z. Abou-Chadi, "Enhancing robustness of digital image watermarks using contourlet transform," in *Proc. 16th IEEE Int. Conf. Image Process. (ICIP)*, Nov. 2009, pp. 3645–3648.

[31] A. Kumar and V. Kumar, "Blind watermarking in contourlet domain with improved detection," *Int. J. Multimedia Appl. (IJMA)*, vol. 3, no. 1, pp. 122–131, 2011.

[32] S. Ghannam and F. Abou-Chadi, "Contourlet versus wavelet transform: A performance study for a robust image watermarking," in *Proc. Int. Conf. Image Vis. Comput. (IVCNZ)*, 2009, pp. 545–500.

[33] M. A. Akhaee, S. M. E. Sahraeian, and F. Marvasti, "Contourlet-based image watermarking using optimum detector in a noisy environment," *IEEE Trans. Image Process.*, vol. 19, no. 4, pp. 967–980, Apr. 2010.

[34] H. V. Poor, *An Introduction to Signal Detection and Estimation*, 2nd ed. New York, NY, USA: Springer-Verlag, 1994.

[35] H. Rabbani, "Image denoising in steerable pyramid domain based on a local laplace prior," *Pattern Recognit.*, vol. 42, no. 9, pp. 2181–2193, 2009.

[36] A. Mairgiotis, G. Chantas, N. Galatsanos, K. Blekas, and Y. Yang, "New detectors for watermarks with unknown power based on student-t image priors," in *Proc. IEEE 9th Workshop Multimedia Signal Process.*, Oct. 2007, pp. 353–356.

[37] D. D.-Y. Po and M. N. Do, "Directional multiscale modeling of images using the contourlet transform," *IEEE Trans. Image Process.*, vol. 15, no. 6, pp. 1610–1620, Jun. 2006.

[38] H. Qu and Y. Peng, "Contourlet coefficient modeling with generalized Gaussian distribution and application," in *Proc. Int. Conf. Audio, Lang., Image Process. (ICALIP)*, Jul. 2008, pp. 531–535.

[39] M. N. Do, "Directional multiresolution image representations," Ph.D. dissertation, School Comput. Commun. Sci., Swiss Federal Inst. Technol. Lausanne, Lausanne, Switzerland, 2001.

[40] M. N. Do and M. Vetterli, "The contourlet transform: An efficient directional multiresolution image representation," *IEEE Trans. Image Process.*, vol. 14, no. 12, pp. 2091–2106, Dec. 2005.

[41] H. Rabbani, M. Vafadust, S. Gazor, and I. Selesnick, "Image denoising employing a bivariate Cauchy distribution with local variance in complex wavelet domain," in *Proc. 12th-Signal Signal Process. Edu. Workshop, 4th Digital Signal Process. Workshop*, Sep. 2006, pp. 203–208.

[42] H. Rabbani, M. Vafadust, and S. Gazor, "Video denoising based on a bivariate Cauchy distribution in 3D complex wavelet domain," in *Proc. 9th Int. Symp. Signal Process. Appl. (ISSPA)*, Feb. 2007, pp. 1–4.

[43] R. Kwitt, P. Meerwald, and A. Uhl, "Color-image watermarking using multivariate power-exponential distribution," in *Proc. 16th IEEE Int. Conf. Image Process. (ICIP)*, Nov. 2009, pp. 4245–4248.

[44] I. W. Selesnick, R. G. Baraniuk, and N. C. Kingsbury, "The dual-tree complex wavelet transform," *IEEE Signal Process. Mag.*, vol. 22, no. 6, pp. 123–156, Nov. 2005.

[45] E. J. Candès and D. L. Donoho, "Ridgelets: A key to higher-dimensional intermittency?" *Philosoph. Trans. Roy. Soc. London A*, vol. 357, no. 1760, pp. 2495–2509, 1999.

[46] E. J. Candès and D. L. Donoho, "Curvelets—A surprisingly effective non-adaptive representation for objects with edges," in *Curve and Surface Fitting*, C. R. A. Cohen and L. Schumaker, Eds. Nashville, TN, USA: Vanderbilt Univ. Press, 2000.

[47] E. J. Candès and D. L. Donoho, "New tight frames of Curvelets and optimal representations of objects with piecewise C^2 singularities," *Commun. Pure Appl. Math.*, vol. 57, no. 2, pp. 219–266, 2004.

[48] C. Nikias and M. Shao, *Signal Processing With Alpha-Stable Distributions and Applications*. New York, NY, USA: Wiley, 1995.

[49] R. Adler, R. Feldman, and M. Taqqu, *A Guide to Heavy Tails; Statistical Techniques and Applications*. Boston, MA, USA: Birkhauser, 1998.

[50] D. Mouchel, "Stable distributions in statistical inference," Ph.D. dissertation, Dept. Statist., Yale Univ., New Haven, CT, USA, 1971.

[51] C. Deng, H. Zhu, and S. Wang, "Curvelet domain watermark detection using alpha-stable models," in *Proc. 5th Int. Conf. Inform. Assurance Security (IAS)*, Aug. 2009, pp. 313–316.

[52] J. P. Nolan, "Maximum likelihood estimation and diagnostics for stable distributions," Ph.D. dissertation, Dept. Math. Statist., American Univ., Washington, DC, USA, 1999.

[53] J. P. Nolan, *Information On Stable Distributions*. [Online]. Available: http://academic2.american.edu/~jpnolan/stable/stable.html.

[54] S. Mittnik, S. T. Rachev, T. Doganoglu, and D. Chenyao, "Maximum likelihood estimation of stable Paretian models," *Math. Comput. Model.*, vol. 29, nos. 10–12, pp. 275–293, 1999.

[55] A. Papoulis, *Probability, Random Variables, and Stochastic Processes*. New York, NY, USA: McGraw-Hill, 1991.

[56] S. M. Kay, *Fundamentals of Statistical Signal Processing, Volume II: Detection Theory*, 1st ed. Englewood Cliffs, NJ, USA: Prentice-Hall, 1998.

[57] *Online Image Database*. [Online]. Available: http://decsai.ugr.es/cvg/dbimagenes/index.php, accessed Mar. 2013.

Hamidreza Sadreazami (S'09) received the B.Sc. degree in electrical engineering from Khaje Nasir Toosi University, Tehran, Iran, in 2007, and the M.Sc. degree in electrical engineering from Shahid Beheshti University, Tehran, in 2010. He is currently pursuing the Ph.D. degree in electrical and computer engineering with Concordia University, Montreal, QC, Canada. He has been a Research Associate with the Signal Processing Group, Concordia University, since 2011, where he has been involved in statistical modeling with applications on image watermarking and image denoising. His research area includes image and video processing using statistical modeling, medical image denoising, and data hiding. He has served as a reviewer for several IEEE journals and major conferences.

M. Omair Ahmad (S'69–M'78–SM'83–F'01) received the B.Eng. degree in electrical engineering from Sir George Williams University, Montreal, QC, Canada, and the Ph.D. degree in electrical engineering from Concordia University, Montreal, QC, Canada. From 1978 to 1979, he was a Faculty Member with New York University College, Buffalo, NY, USA. In 1979, he joined the faculty of Concordia University as an Assistant Professor of Computer Science. He joined the Department of Electrical and Computer Engineering, Concordia University, where he was the Chair with the Department from 2002 to 2005, and is currently a Professor. He is the Concordia University Research Chair (Tier I) in Multimedia Signal Processing. He has authored in the area of signal processing and holds four patents. His current research interests include the areas of multidimensional filter design, speech, image and video processing, nonlinear signal processing, communication DSP, artificial neural networks, and VLSI circuits for signal processing. He was a Founding Researcher with Micronet Company, Ltd., Sapporo, Japan, as a Canadian Network of Centers of Excellence from 1990 to 2004. Previously, he was an Examiner of the order of Engineers of Quebec. He was an Associate Editor of the IEEE TRANSACTIONS ON CIRCUITS AND SYSTEMS PART I: FUNDAMENTAL THEORY AND APPLICATIONS from 1999 to 2001. He was the Local Arrangements Chairman of the 1984 IEEE International Symposium on Circuits and Systems. In 1988, he was a member of the Admission and Advancement Committee of the IEEE. He has served as the Program Co-Chair for the 1995 IEEE International Conference on Neural Networks and Signal Processing, the 2003 IEEE International Conference on Neural Networks and Signal Processing, and the 2004 IEEE International Midwest Symposium on Circuits and Systems. He was a General Co-Chair of the 2008 IEEE International Conference on Neural Networks and Signal Processing. He is the Chair of the Montreal Chapter IEEE Circuits and Systems Society. He was a recipient of numerous honors and awards, including the Wighton Fellowship from the Sandford Fleming Foundation, an induction to Provosts Circle of Distinction for Career Achievements, and the Award of Excellence in Doctoral Supervision from the Faculty of Engineering and Computer Science, Concordia University.

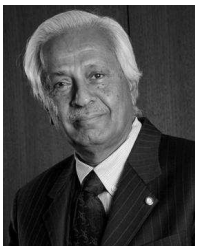

M. N. S. Swamy (S'59–M'62–SM'74–F'80) received the B.Sc. (Hons.) degree in mathematics from the University of Mysore, Mysore, India, in 1954, the Diploma degree in electrical communication engineering from the Indian Institute of Science, Bangalore, India, in 1957, and the M.Sc. and Ph.D. degrees in electrical engineering from the University of Saskatchewan, Saskatoon, SK, Canada, in 1960 and 1963, respectively. He was an Honorary Professor with National Chiao Tong University, Hsinchu, Taiwan, in 2009. He is currently a Research Professor and the Director of the Center for Signal Processing and Communications with the Department of Electrical and Computer Engineering, Concordia University, Montreal, QC, Canada, where he served as the Chair of the Department of Electrical Engineering from 1970 to 1977, and the Dean of Engineering and Computer Science from 1977 to 1993. During that time, he developed the faculty into a research-oriented one from what was primarily an undergraduate faculty. Since 2001, he has been the Concordia Chair (Tier I) in Signal Processing. He has also taught with the Department of Electrical Engineering, Technical University of Nova Scotia, Halifax, NS, Canada, the University of Calgary, Calgary, AB, Canada, and the Department of Mathematics, University of Saskatchewan. He has published in the areas of number theory, circuits, systems, and signal processing, and holds five patents. He has co-authored six books and three book chapters. He was a Founding Member of Micronet Company, Ltd., Sapporo, Japan, as a Canadian Network of Centers of Excellence from 1990 to 2004, and also its Coordinator of Concordia University. He is a fellow of the Institute of Electrical Engineers, U.K, the Engineering Institute of Canada, the Institution of Engineers, India, and the Institution of Electronic and Telecommunication Engineers, India. In 2008, Concordia University instituted the M.N.S. Swamy Research Chair in Electrical Engineering as a recognition of his research contributions. He was inducted in 2009 to the Provosts Circle of Distinction for career achievements. He has served the IEEE in various capacities such as the President Elect in 2003, President in 2004, Past-President in 2005, Vice President (publications) from 2001 to 2002, Vice President in 1976, Editor-in-Chief of the IEEE TRANSACTIONS ON CIRCUITS AND SYSTEMS I from 1999 to 2001, Associate Editor of the IEEE TRANSACTIONS ON CIRCUITS AND SYSTEMS from 1985 to 1987, Program Chair of the 1973 IEEE CAS Symposium, General Chair of the 1984 IEEE CAS Symposium, Vice Chair of the 1999 IEEE Circuits and Systems (CAS) Symposium, and a member of the Board of Governors of the CAS Society. He was a recipient of many IEEE-CAS Society awards, including the Education Award in 2000, the Golden Jubilee Medal in 2000, and the 1986 Guillemin-Cauer Best Paper Award. He has been the Editor-in-Chief of the journal *Circuits, Systems and Signal Processing (CSSP)* since 1999. Recently, CSSP has instituted the Best Paper Award in his name.